Multidisciplinary Design Optimization of Low-Boom Supersonic Aircraft with Mission Constraints

Wu Li* and Karl Geiselhart†
NASA Langley Research Center, Hampton, Virginia 23681, USA

Design of low-boom supersonic aircraft is heavily dictated by aircraft volume and lift distributions. These unique design characteristics make it a challenge to enforce mission requirements (such as static margins and trim requirements) during design optimization. This low-boom design challenge is resolved by using reversed equivalent area targets for low-fidelity low-boom design and a decomposition method for multidisciplinary design optimization (MDO). The corresponding low-boom MDO problem includes aircraft mission constraints for cruise ranges, cruise speeds, trim margin for low-boom cruise, static margins for takeoff/cruise/landing, tail rotation angles for trim at takeoff/landing, takeoff/landing field lengths, and approach velocity, as well as volume constraints for cabin and main landing gear packaging. The decomposition method is developed to optimally resolve the conflicts between the low-boom design objective and other design constraints. The decomposition method is successfully applied to design a low-boom supersonic configuration that carries 40 passengers, has low-boom cruise of Mach 1.6 with range ≥ 2,500 nm, and can also cruise at Mach 1.8 with range ≥ 3,600 nm. The generated configuration satisfies all specified mission constraints and has the potential to achieve a low-boom ground noise level below 75 PLdB.

Nomenclature

A_e	=	classical equivalent area (ft^2) defined by Mach angle cut method
$A_{e,r}$	=	reversed equivalent area (ft^2) defined by using reverse propagation of off-body pressure
$A_{new,e}$	=	A_e (ft^2) of new configuration
$A_{new,e}^{lift}$	=	A_e (ft^2) of new configuration due to lift
$A_{0,e,r}^{target}$	=	$A_{e,r}$ target (ft^2) for baseline configuration
$A_{new,e,r}^{target}$	=	$A_{e,r}$ target (ft^2) for new configuration
$A_{new,e}^{volume}$	=	A_e (ft^2) of new configuration due to volume
c_i	=	chord length (ft) of airfoil at span location y_i
c_{root}	=	chord length (ft) of root airfoil of horizontal tail
c_{tip}	=	chord length (ft) of tip airfoil of horizontal tail
D	=	design vector for optimization
D_0	=	design vector for baseline configuration
D_{new}	=	design vector for new configuration
d_i	=	width parameter (ft) for fuselage cross section at x_i
f	=	objective function for optimization
g_i	=	constraint function for optimization
i, m	=	indices
l	=	lower bound vector for design vector D
$MTOGW_{fea}$	=	Maximum takeoff gross weight estimate from FEA-based analysis
$MTOGW_{flops}$	=	Maximum takeoff gross weight estimate from FLOPS weight analysis
s_i	=	sectional span length (ft) of i-th wing section
u	=	upper bound vector for design vector D
W_0	=	start cruise weight (lb) of baseline configuration
$W_{fuse,fea}$	=	fuselage weight estimate from FEA-based analysis

* Senior Research Engineer, Aeronautics Systems Analysis Branch
† Aerospace Engineer, Aeronautics Systems Analysis Branch

$W_{fuse,flops}$ = fuselage weight estimate from FLOPS weight analysis
W_{new} = start cruise weight (lb) of new configuration
$W_{wing,fea}$ = wing structural weight estimate from FEA-based analysis
$W_{wing,flops}$ = wing structural weight estimate from FLOPS weight analysis
x, y, z = coordinates (ft) of point in space
$x_{0,e}$ = effective length (ft) of baseline configuration, which is the largest effective distance where Mach angle cut plane intersects the configuration
$x_{0,limit}$ = upper limit (ft) of effective distance for calculating A_e matching error of baseline configuration
x_{aft} = x coordinate (ft) of trailing edge of root airfoil of wing
x_e = effective distance (ft) for A_e calculation
$x_{e,limit}$ = upper limit (ft) of effective distance for calculating A_e matching error
$x_{e,MR}$ = effective distance location (ft) where $A_{e,r}$ and A_e start to deviate from each other
x_{frt} = x coordinate (ft) of leading edge of root airfoil of wing
x_i = x coordinate (ft) of fuselage cross section location
$x_{new,e}$ = effective length (ft) of new configuration
$x_{new,limit}$ = upper limit (ft) of effective distance for calculating A_e matching error of new configuration
x_{tip} = x coordinate (ft) of trailing edge of tip airfoil of wing
y_i = y coordinate (ft) of wing span location
$\delta_{i,max}$ = camber-line designation, fraction of chord from leading edge over which design load is uniform, for NACA 63-series airfoil at span location y_i
δ_{max} = camber-line designation, fraction of chord from leading edge over which design load is uniform, for NACA 63-series airfoil
θ_{htail} = deflection angle (degree) of an all-moving horizontal tail at cruise
θ_i = twist angle (degree) of airfoil at span location y_i
λ_{fuse} = calibration factor for fuselage weight estimate
λ_{wing} = calibration factor for wing structural weight estimate
$\tau_{i,max}$ = design section lift coefficient for NACA 63-series airfoil at span location y_i
τ_{max} = design section lift coefficient for NACA 63-series airfoil

I. Introduction

DESIGN of low-boom supersonic aircraft is heavily dictated by aircraft volume and lift distributions. Because lift distributions from low-fidelity aerodynamics and computational fluid dynamics (CFD) are significantly different, it is necessary to use CFD for low-boom design. Automation of Euler CFD analysis has been successfully completed for aircraft conceptual design [1-3]. Euler CFD analysis is routinely used for analysis and design of low-boom supersonic configurations [4]. CFD-based low-boom design methods can be successfully applied to reduce the undertrack ground noise level of a supersonic configuration to approximately 78 PLdB [5-9] and the Cart3D adjoint low-boom design method has the potential to reduce the ground noise level further [10,11]. But, for any realistic design of supersonic aircraft, it is necessary to include other design objectives and/or mission constraints [12-21].

In theory, the low-boom characteristics of a supersonic aircraft are very sensitive to its outer mold line (OML) and surface pressure distribution at cruise. Any significant alteration of its OML (including control surface deflections) at the cruise altitude could have a detrimental effect on its low-boom characteristics. Tables 5 and 6 in Ref. [22] quantify the variability of the perceived loudness of ground noise due to the control surface deflections during cruise flight of a low-boom flight demonstrator. For a well-designed low-boom configuration, it is generally necessary to use fuel redistributions to maintain a level flight with the designed low-boom OML instead of using control surface deflections. This leads to one of the most difficult design constraints for low-boom supersonic aircraft: matching the center of aerodynamic pressure to the center of gravity (CG) in the longitudinal direction with fuel redistributions during cruise flight. This trim constraint for low-boom supersonic aircraft is also largely determined by the aircraft volume and lift distributions. Methods were developed to incorporate the trim constraint in the low-boom target for reversed equivalent area ($A_{e,r}$) [5] and they were used successfully for CFD-based design of two low-boom supersonic configurations [7,8]. But, these methods are computationally too expensive and not applicable during preliminary conceptual design when mission constraints are included in optimization. A conceptual design approach of incorporating the trim constraint in the low-boom F-function target of a wing-body configuration [23] needs to be further verified by using an aircraft configuration with nacelles and tails. In this paper, a decomposition method for low-fidelity multidisciplinary design optimization (MDO) is proposed to generate a low-boom supersonic concept that

has the potential to achieve a low-boom ground noise level below 75 PLdB and satisfies twelve mission constraints including the low-boom trim constraint.

As the low-boom design technology evolves over time, the classical low-fidelity low-boom design methods for equivalent area (A_e) matching become obsolete because the end value of A_e is usually significantly lower than the end value of $A_{e,r}$ calculated from CFD near-field pressure distribution [5]. (The end value of A_e is the value of A_e at the effective length of the configuration as shown in Fig. 1.) Note the difference of end values of $A_{e,r}$ and A_e of a 100 ft low-boom supersonic demonstrator concept in Fig. 1, which is a superposition of Figs. 9 and 10 in Ref. [8]. Any target that has the same end value as A_e cannot be matched by $A_{e,r}$ using CFD-based boom analysis; so such an A_e target is irrelevant to any CFD-based low-boom design. The method of increasing the end value of an A_e target for low-fidelity low-boom design was first applied to design of a low-boom supersonic business jet and two low-boom wind tunnel models [12,24].

With CFD-based boom analysis, it becomes clear that A_e agrees with $A_{e,r}$ up to an effective distance location $x_{e,MR}$ (usually in the aft part of the wing before the nacelles, cf. Fig. 1). That is, the classical sonic boom theory of treating a supersonic configuration as a body of revolution is valid for a wing-body configuration but fails once nacelles are included in sonic boom analysis. The required increment of the end value of an A_e target for low-fidelity low-boom design can be calculated by using the end value of $A_{e,r}$. A successful match of the low-fidelity A_e to an $A_{e,r}$ target while satisfying the specified mission constraints ensures the feasibility of a CFD-based low-boom configuration that approximately satisfies the same mission constraints.

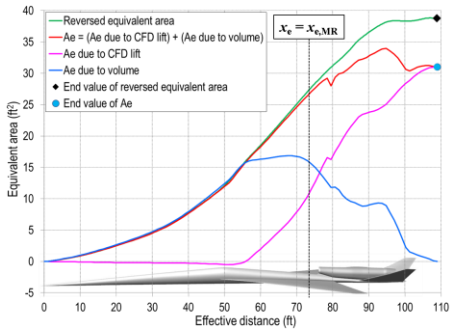

Fig. 1 Comparison of $A_{e,r}$ and A_e.

The mathematical theory for matching the low-fidelity A_e to an $A_{e,r}$ target can be described as follows. Assume that the low-fidelity A_e of a configuration matches the $A_{e,r}$ target up to $x_{e,MR}$. Even though the A_e distributions due to lift from low-fidelity aerodynamics and CFD could be very different, the low-fidelity lift A_e can be used as a target to be matched by the CFD lift A_e with wing camber tailoring. This tailoring has a minimum effect on the volume A_e. So the CFD A_e of the resulting configuration matches the $A_{e,r}$ target up to $x_{e,MR}$. Further CFD-based aft tailoring of cambers of aerodynamic surfaces behind $x_{e,MR}$ could be used to match the $A_{e,r}$ target for a CFD-based low-boom design. The final CFD-based low-boom design has the same lift distribution as the low-fidelity one on the effective distance interval [0, $x_{e,MR}$]. Because the longitudinal CG of the aircraft is usually in [0, $x_{e,MR}$], the final low-boom design has the same longitudinal lift distribution as the low-fidelity design on one side of the longitudinal CG of the aircraft. This allows the final low-boom design to approximately retain the longitudinal pressure center and trim margin of the low-fidelity design, as well as the cruise static margin (SM). As a result, the CFD-based trim and static margin constraints can be traded with the low-boom objective during the low-fidelity low-boom design process, which is a much easier problem to solve and allows better design trades for performance, weight, stability, and low-boom objective.

The MDO problem for conceptual design of low-boom supersonic aircraft with mission constraints can be written as a standard nonlinear optimization problem.

$$\min_{D} f(D) \text{ subject to } g_i(D) \le 0 \text{ for } 1 \le i \le m \text{ and } l \le D \le u \tag{1}$$

The design vector D is a collection of design variables for fuselage cross sections, wing planform shape, airfoil camber and design lift parameters, horizontal tail planform shape, engine thrust, main landing gear location, and control surface deflection angles. The objective function $f(D)$ is usually the error between an $A_{e,r}$ target and aircraft low-fidelity A_e over an effective distance interval [0, $x_{e,limit}$]. The value of $x_{e,limit}$ depends on D and is determined to ensure that $A_{e,r}$ and A_e are totally unrelated for effective distances after $x_{e,limit}$. For this paper, two range requirements are automatically satisfied by the fixed-range mission analysis: a range of 2,500 nm for low-boom mission at cruise Mach 1.6, and a

range of 3,200 nm (which will be changed to 3,600 nm later) for overwater mission at cruise Mach 1.8. Ten constraints (m = 10) for the following mission performance parameters are included in the optimization: low-boom trim margin, takeoff/cruise/landing static margins, landing and takeoff (LTO) field lengths, approach velocity, longitudinal offset of main landing gear location from empty weight CG, and tail rotation angles for trim at LTO. Volume constraints for 40 passenger seats and main landing gear packaging are enforced by the lower bound vector l. The cruise Mach number for the low-boom mission, number of passengers, and range for the overwater mission are based on an unpublished economic feasibility study for supersonic transports. The cruise Mach 1.8 for the overwater mission is based on LTO noise, emissions, and technology availability. The range for the low-boom mission is limited by the maximum cruise weight allowed by the requirement for a low-boom ground noise level less than 75 PLdB. The LTO field lengths, approach velocity, and maximum vehicle length are determined by the relevant service airports. A more comprehensive conceptual design of low-boom supersonic aircraft might use more constraints, but the given set of constraints includes the most significant constraints that could conflict with the low-boom design objective. The analyses involved in the objective and constraint evaluations include propulsion, aerodynamics, aircraft weights estimation, mission and LTO performance, stability, equivalent area, sonic boom propagation, and ground signature loudness. See Ref. [25] for details about these analyses.

The paper is organized as follows. Section II documents the low-boom MDO problem and its solution method. In Section III, the MDO solution method is applied to design a low-boom supersonic transport with the mission constraints described above. The final section includes the concluding remarks.

II. MDO for Low-Boom Supersonic Concepts

In practice, an MDO solution process requires tremendous efforts to set up. The data links among different disciplinary analysis codes are complex, and the data consistency is difficult to verify. Moreover, empirical design knowledge is necessary for many implicit assumptions used to define the MDO problem. In the following subsections, the key issues related to setting up and solving the low-boom MDO problem are discussed.

A. Mission Constraints

The speed and range constraints are mainly based on a preliminary economic feasibility study, which indicates that a supersonic transport is economically viable if it can carry 40 passengers, fly a minimum range of 2,500 nm for a low-boom mission at cruise Mach 1.6, and also fly a minimum range of 3,200 nm (which will be changed to 3,600 nm later) for an overwater mission at cruise Mach 1.8. Using the fixed-range mission analysis, these speed and range constraints are automatically satisfied. The requirement for 40 passengers is enforced with fuselage volume constraints and payload weight. The fuselage volume constraints are satisfied by using lower bounds on the fuselage cross section widths. The cruise altitude selection is based on trades between performance and low-boom benefits. For a given low-boom vehicle, lower cruise altitudes result in lower ground noise levels but reduced performance. So, the cruise altitude for the low-boom mission is set at 45,000 ft for the maximum low-boom benefit while avoiding the cruise altitude range for subsonic transports. The cruise altitude for the overwater mission is limited to 60,000 ft for maximum performance benefit allowed by the engine.

With the fixed-range mission analysis, two range constraints are eliminated from the MDO problem formulation. The remaining ten mission constraints are defined as follows.

(II.A.1) Low-boom trim margin ≥ 1 ft (i.e., with fuel redistributions, the longitudinal CG can be placed at least 1 ft ahead of the center of aerodynamic pressure at the start cruise condition for the low-boom mission)
(II.A.2) Main landing gear location constraint ≥ 4 ft (i.e., the main landing gear longitudinal location is at least 4 ft behind the longitudinal CG of the aircraft at empty weight)
(II.A.3) Cruise static margin for the low-boom mission ≥ 2%
(II.A.4) Takeoff static margin ≥ 2%
(II.A.5) Landing static margin ≥ 2%
(II.A.6) Takeoff field length ≤ 8,300 ft
(II.A.7) Landing field length ≤ 8,300 ft
(II.A.8) Tail rotation angle for trim at takeoff ≥ -20°
(II.A.9) Tail rotation angle for trim at landing ≥ -20°
(II.A.10) Approach velocity ≤ 150 knots

B. Equivalent Area Target Scaling for Low-Boom Design Objective

The prevailing low-boom optimization approach is to minimize the difference between a low-boom target and relevant $A_{e,r}$ or near-field pressure distribution of the aircraft configuration. For any given low-boom target, it is

impossible to know *a priori* whether it can be matched by a configuration with a given cruise weight at a specified cruise altitude. So, it is not uncommon to find no desirable solution to the low-boom design problem after repeated trials when the cruise lift constraint is imposed or a low-boom solution is found for a significantly different cruise weight.

If the aircraft weight and CG analyses are included in low-boom design, then the start cruise weight changes with design modifications. A fixed maximum takeoff gross weight (MTOGW) might make the low-boom design problem unnecessarily more difficult because any excess MTOGW leads to a heavier aircraft at the start cruise, which usually means worse boom characteristics.

An additional challenge for low-fidelity low-boom design arises due to the potentially significant differences between low-fidelity A_e and CFD-based $A_{e,r}$, which could render the low-fidelity low-boom design completely irrelevant to the CFD-based low-boom design.

A solution to these design challenges is the use of scaled $A_{e,r}$ targets for low-fidelity low-boom design. For this method, assume that a baseline configuration D_0 has a start cruise weight W_0 (from the mission analysis) at a specified cruise altitude. First, compute its $A_{e,r}$ and determine its effective length $x_{0,e}$. Generate an $A_{e,r}$ target $A_{0,e,r}^{\text{target}}$ for the baseline. Determine an upper bound $x_{0,\text{limit}}$ of effective distance for A_e matching error calculation near $x_{e,\text{MR}}$ (cf. Fig. 1). Then, scale the $A_{e,r}$ target for any new configuration, as follows. For any modified configuration D_{new}, let W_{new} be its start cruise weight and $x_{\text{new,e}}$ its effective length. Then the following scaled reversed equivalent area target $A_{\text{new,e,r}}^{\text{target}}$ will be used to define the low-boom objective for D_{new}.

$$A_{\text{new,e,r}}^{\text{target}}(x_e) = \frac{W_{\text{new}}}{W_0} \cdot A_{0,e,r}^{\text{target}}\left(\frac{x_{0,e}}{x_{\text{new,e}}} \cdot x_e\right) \tag{2}$$

The low-boom objective for D_{new} is the matching error between $A_{\text{new,e,r}}^{\text{target}}$ and $A_{\text{new,e}}$ over the effective distance interval $[0, x_{\text{new,limit}}]$, where

$$x_{\text{new,limit}} = \frac{x_{\text{new,e}}}{x_{0,e}} \cdot x_{0,\text{limit}} \tag{3}$$

The low-boom objective function $f(D_{\text{new}})$ can be defined by the maximum absolute difference or integral of the squares of differences between $A_{\text{new,e,r}}^{\text{target}}$ and $A_{\text{new,e}}$. That is,

$$f(D_{\text{new}}) = \max_{0 \le x_e \le x_{\text{new,limit}}} \left|A_{\text{new,e,r}}^{\text{target}}(x_e) - A_{\text{new,e}}(x_e)\right| \tag{4}$$

or

$$f(D_{\text{new}}) = \left(\frac{1}{x_{\text{new,limit}}} \cdot \int_0^{x_{\text{new,limit}}} \left|A_{\text{new,e,r}}^{\text{target}}(x_e) - A_{\text{new,e}}(x_e)\right|^2 dx_e\right)^{\frac{1}{2}} \tag{5}$$

The scaling allows the reversed equivalent area target $A_{\text{new,e,r}}^{\text{target}}$ to have approximately the same effective length and end value as the $A_{e,r}$ for D_{new}. In theory, the predicted effective length and end value for $A_{e,r}$ are accurate if D_{new} is close to the baseline D_0. In practice, it might be necessary to update $A_{0,e,r}^{\text{target}}$, W_0, $x_{0,e}$, and $x_{0,\text{limit}}$ using the analysis results of the newly generated design D_{new} during optimization iterations to improve the approximation accuracy.

C. Analysis Dependencies for Low-Fidelity Low-Boom Design

Figure 2 is a flowchart for the dependencies among the multidisciplinary analyses used to compute the objective and constraint values for a supersonic aircraft concept. Details for the involved analysis codes were documented in Ref. [25], except that the low-boom target scaling and objective are defined in the preceding subsection.

The highlighted yellow block is a coupled weight and mission analysis. To start a fixed-range mission analysis, the zero fuel weight must be specified, which is generated by the aircraft weights estimation analysis. But, one key input for the aircraft weights estimation analysis is MTOGW, which is an output of the fixed-range mission analysis. So, an iteration process is required to ensure that the MTOGW generated by the fixed-range mission analysis equals the MTOGW used for the aircraft weights estimation. An alternative approach is to fix the MTOGW for both analyses. Then the range becomes an output of the mission analysis and a constraint must be used to satisfy each minimum range requirement, which makes the optimization problem more difficult to solve. The iterations for MTOGW ensure

that the range constraint is satisfied with the minimum MTOGW. It usually takes a few iterations to get a converged MTOGW, so the coupled weight and mission analysis can be completed efficiently. The minimum range requirements for the two missions (specified in Subsection II.A) lead to two MTOGW values. The maximum of two MTOGW values from the dual mission analysis is used for the weights estimation. This approach limits the influence of the overwater mission only to the MTOGW and maximum speed for the aircraft weights estimation.

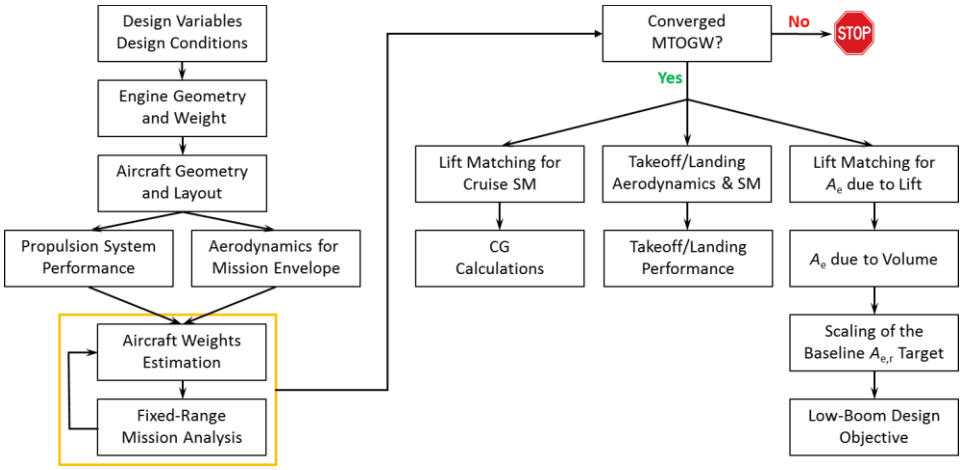

Fig. 2 Dependencies among multidisciplinary analyses of supersonic aircraft concept.

No matter which mission analysis option is used, insufficient thrust and/or poor aerodynamic performance could lead to failure of the mission analysis. For each failed case, no further analysis is required (cf. the stop sign in Fig. 2); predetermined infeasible constraint values and high objective value are used for the current design so that the optimization algorithm will move away from designs with failed mission analyses.

After the coupled weight and mission analysis, the start cruise weight for the low-boom mission determines the remaining analyses for the low-boom cruise flight and the converged MTOGW is used in LTO analyses. The two lift matching boxes in Fig. 2 are for two different analysis codes to match the lift for the start cruise weight.

D. Calibration of Empirical Aircraft Weights by FEA-based Weight Estimates

The aircraft weights estimation is critical for the low-boom design process, because the converged MTOGW and start cruise weight for the low-boom mission determine the takeoff/cruise/landing analyses. To make the low-fidelity low-boom design process more reliable, an FEA-based weights estimation method [26] is used to calibrate the aircraft weights estimation [27] in Flight Optimization System (FLOPS) [28] so that the calibrated FLOPS aircraft weights estimation is an accurate approximation of the FEA-based weights estimation. Figure 3 is a flowchart about how the estimated wing/fuselage weights and MTOGW are updated in the calibration process.

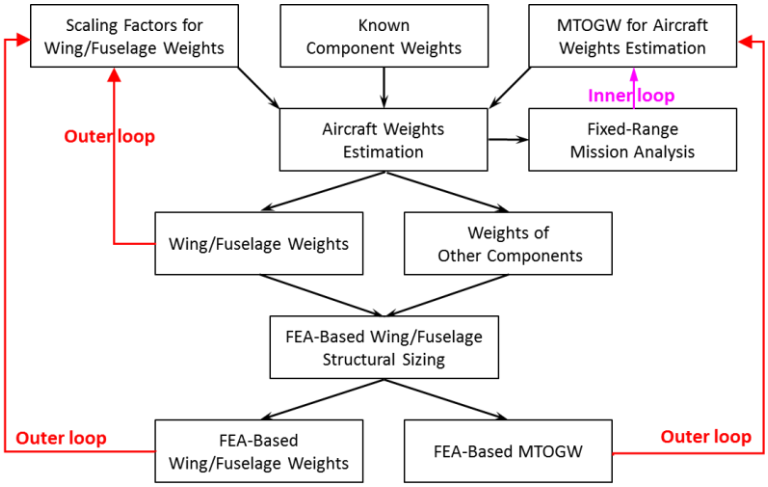

Fig. 3 Calibration of FLOPS weights estimation by FEA-based weights estimation.

The goal of this calibration process is to find the wing and fuselage weight scaling factors used in the FLOPS weights estimation such that the FLOPS wing and fuselage weights are approximately equal to the FEA-based wing and fuselage weights, respectively, for a baseline configuration.

The pink arrow in Fig. 3 completes the inner iteration loop for a converged MTOGW between the FLOPS weights estimation and fixed-range mission analysis. The red arrows in Fig. 3 complete the outer iteration loop for a converged MTOGW between the FLOPS weights estimation and FEA-based weights estimation. The outer iteration loop also finds the calibrated weight scaling factors for wing and fuselage that make the FLOPS wing and fuselage weights equal the FEA-based wing and fuselage weights. Here are the updating formulas for the outer loop in Fig. 3.

$$\frac{W_{\text{fuse,fea}}}{W_{\text{fuse,flops}}} \cdot \lambda_{\text{fuse}} \mapsto \lambda_{\text{fuse}} \tag{6}$$

$$\frac{W_{\text{wing,fea}}}{W_{\text{wing,flops}}} \cdot \lambda_{\text{wing}} \mapsto \lambda_{\text{wing}} \tag{7}$$

$$\text{MTOGW}_{\text{fea}} = \text{MTOGW}_{\text{flops}} - \left(W_{\text{wing,flops}} - W_{\text{wing,fea}} + W_{\text{fuse,flops}} - W_{\text{fuse,fea}}\right) \tag{8}$$

$\text{MTOGW}_{\text{fea}}$ given in Eq. (8) is used as the initial guess for MTOGW in the inner iteration loop (cf. Subsection II.C). The iteration process terminates when the FLOPS wing and fuselage weights are approximately equal to the FEA-based wing and fuselage weights, respectively.

If the iteration process terminates successfully, then the mission analysis, FLOPS weights estimation, and FEA-based weights estimation are performed using the same MTOGW. Moreover, the FEA-based weights estimation and FLOPS have the same estimates for wing and fuselage weights.

For the FLOPS weights estimation used in this paper, the FEA-based calibration factors λ_{fuse} and λ_{wing} are 0.8 and 1, respectively. The calibrated FLOPS estimation of fuselage weight is its default estimate scaled by λ_{fuse}. For wing structural weight, the FLOPS default structural weight estimate scaled by λ_{wing} is used as the calibrated FLOPS wing structural weight. In theory, by using appropriate values of λ_{fuse} and λ_{wing}, FLOPS can match any given wing and fuselage weights.

E. Baseline Geometry and Design Variables

An OpenVSP [29] baseline geometry is constructed using some empirical knowledge about feasible low-boom supersonic transports. A parametric study of equivalent area targets shows that a supersonic configuration with a length of 242 ft has the potential to carry 40 passengers, cruise at Mach number of 1.6 and altitude of 45,000 ft, and achieve a low-boom ground noise level below 75 PLdB. This determines the fuselage length of 242 ft. The fuselage shape has a side view similar to Concorde (cf. [30] for a brief account of how Concorde evolved from a research project to a real vehicle). The fuselage is parameterized by seven width parameters (d_1, …, d_7) at the cross section locations (x_1, …, x_7) and four cross section location parameters (x_1, x_2, x_3, x_4) (cf. Fig. 4).

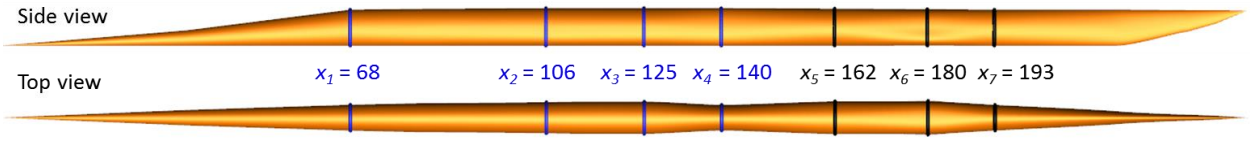

Fig. 4 Baseline fuselage OML and its parameterized cross sections.

A cross section height of 7.3 ft is used for the passenger cabin approximately from x = 95 ft to 175 ft. The fuselage cross section widths are minimized while maintaining the volume for 40 passenger seats, service area, and storage of main landing gear. The coke bottle shape for the width distribution near x = 140 ft (cf. Fig. 4) is determined by a preliminary wave drag minimization. The volume constraints for the seven width parameters are defined as follows, where the lower bounds are used for the baseline.

$$d_1 \geq 5,\ d_2 \geq 6,\ d_3 \geq 6.2,\ d_4 \geq 5,\ d_5 \geq 6.3,\ d_6 \geq 6.3,\ d_7 \geq 5 \tag{9}$$

Small perturbation ranges for design variables x_1, x_2, x_3, and x_4 are used to make the fuselage volume distribution more flexible to help match a given low-boom $A_{e,r}$ target.

The baseline wing planform (cf. Fig. 5) is mainly determined by the lift distribution requirement for low-boom shaping (i.e., it has the potential to eliminate the differences between the $A_{e,r}$ target and A_e). The wing span is 98 ft and

the wing area is 3775 ft^2. The planform has 5 sections, with the first rectangular section hidden inside the fuselage. The longitudinal locations of the trailing edges (TE) of the three inboard sections are fixed at x = 190 ft. This location is determined by the main landing gear packaging and an attempt to shield the engine inlet shocks. The two outer wing sections form a trapezoidal shape, with an airfoil definition at the span location y_4 for more flexibility in lift tailoring. Nine shape parameters are used to morph the baseline wing planform without creating any undesirable planform shape: the chord length for the rectangular root section (which changes the location x_{frt} of the leading edge (LE) of the root section), x coordinate (x_{tip}) of TE of the tip airfoil, sectional spans for the four outboard sections, and chord lengths at y_2, y_3, and y_5. By forcing $x_{tip} > x_{aft}$, the TE of the outboard wing section has a backward sweep. A monotone decreasing of the chord lengths of the airfoils from inboard to outboard can be easily enforced with bounds on the chord lengths, which ensures the LE sweeps of wing sections are positive. These nine planform parameters define a unique wing planform under the specified shape constraints for the rectangular root section, three fixed inboard TEs, and trapezoidal shape for two outboard sections. This wing planform parametric scheme allows the use of simple bounds on the design variables to define a large design space for the wing planform that does not include any undesirable wing planform shape.

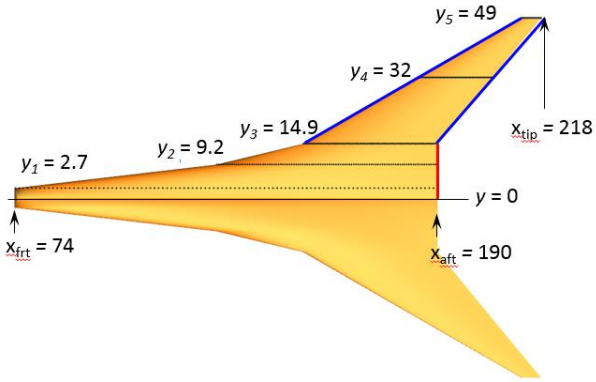

Fig. 5 Baseline wing planform and its parameterized cross sections.

The airfoil thicknesses are based on the available empirical data. The NACA 63-series airfoils [31] are used to define the baseline wing. A camber parameter δ_{max} and design lift parameter τ_{max} (i.e., the parameters A and CLI in the computer code to generate NACA 63-series airfoils [31]) are used to parameterize each airfoil. Eight parameters $\delta_{i,max}$ and $\tau_{i,max}$ for airfoils at the span locations y_i (i=1,2,3,4) are used as design variables. Moreover, the twist angles for airfoils at the span locations y_4 and y_5 are also used as design variables. A total of 10 design variables are available to modify the camber surface of a given wing planform.

The highest possible angle of incidence of the wing with respect to the fuselage is used to minimize the cruise angle of attack. In general, a higher cruise angle of attack results in a shorter effective length of the configuration at cruise and makes it more difficult to attain a low-boom design. An angle of incidence of 1.4° is used for the baseline wing, which is fixed during the low-boom design process.

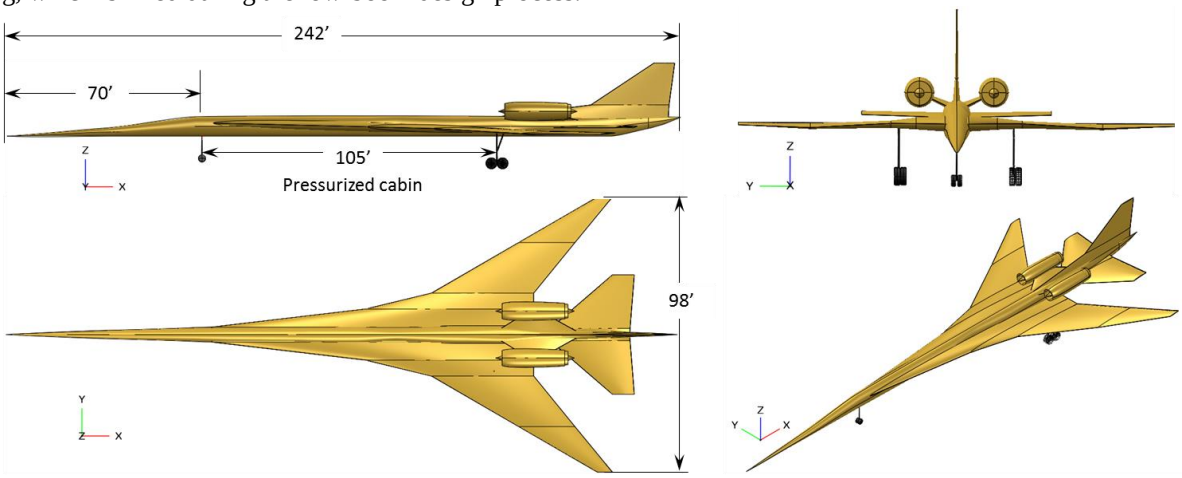

Fig. 6 Baseline configuration.

The standard planform parameters of a trapezoidal horizontal tail are used as the design variables: sweep, span, root chord length, and tip chord length. The deflection angle of the all-moving horizontal tail at cruise is also used as a design variable to trade the amount of the lift carried by the tail. The vertical tail is approximately sized by the lateral control requirement and the pylon is roughly sized for structural integrity. These two components are fixed during the low-boom design process. The nacelle geometry is based on an advanced engine for supersonic transports and is scaled for the required thrust. Figure 6 is the baseline configuration including all geometry components and the landing gear. The pressurized cabin is from x = 70 ft to x =175 ft with a total length of 105 ft.

Table 1 Auxiliary design variables for baseline

Engine thrust = 49,000 lb	LE flap deflection angle for landing = -2°
Main gear longitudinal location = 176 ft	TE flap deflection angle for landing = 10°
Main gear length = 11.5 ft	Longitudinal CG offset for takeoff = 8 ft
TE flap deflection angle for takeoff = 13.7°	Longitudinal CG offset for landing = 8 ft

Eight auxiliary design variables and their values for the baseline are listed in Table 1. The engine thrust affects the mission analysis, engine weight, nacelle size, and LTO field lengths; the main gear location affects the aircraft CG, LTO SMs and field lengths, and fuselage volume constraint for the main gear packaging. The remaining auxiliary design variables are used to satisfy the LTO constraints.

Obviously, if there were an ideal low-boom design that were not included in the design space, any optimization method would fail to find such a solution. In practice, defining the design space is a knowledge-based trial and error process. The exact bounds for the design variables are not specified here, because they are subject to changes after each optimization run. In general, the ranges of design variables are selected to make each geometry design variable of the updated baseline configuration near the mid location if possible, while satisfying the wing planform shape constraints and fuselage volume constraints.

F. Decomposition Method for Low-Boom MDO

Mathematically, the low-fidelity low-boom design problem with the specified mission constraints can be written as Eq. (1). The design vector D is the collection of 43 design variables described in Subsection II.E: 11 fuselage shape parameters, 19 wing shape parameters, 5 horizontal tail shape parameters, and 8 auxiliary parameters. The objective function $f(D)$ is defined by either Eq. (4) or Eq. (5). The constraints $g_i(D) \le 0$ ($1 \le i \le m = 10$) represent the ten mission constraints described in Subsection II.A. A solution of the nonlinear optimization problem is considered as a plausible low-boom design if the A_e matching error is sufficiently small (e.g., less than 3% of the end value). A plausible low-boom design can usually be further shaped using high-fidelity analysis methods to attain a CFD-based low-boom design.

Preliminary trials with a direct optimization solution approach for Eq. (1) did not yield any plausible low-boom designs. That is, the low-boom objective of the best design is not low enough to be considered as plausible. Existing derivative-free optimization algorithms are neither efficient nor effective to solve a nonlinear optimization problem with 43 design variables and 10 nonlinear constraints. Possible multiple local minima make it more difficult to determine the design vector bounds l and u that would contain a global minimum. Moreover, the objective function could be discontinuous due to possible failed mission analyses.

A careful examination of the low-boom design problem reveals that the low-boom MDO problem can be decomposed into the following simpler subproblems: (i) use design exploration to determine the initial values of the auxiliary design variables for a baseline configuration (such as minimizing MTOGW of the baseline with respect to the engine thrust); (ii) use 19 wing design variables and 5 horizontal tail design variables to tailor the lift distribution and reduce the low-boom objective defined by Eq. (4) with the trim constraint; (iii) use 11 fuselage design variables to minimize the low-boom objective defined by Eq. (5) with the trim constraint; (iv) repeat Steps (ii) and (iii) until A_e matching error is fully minimized, with the options of using all geometry design variables simultaneously and/or minimizing the low-boom objective and MTOGW simultaneously; (v) use 6 auxiliary design variables (excluding the main gear longitudinal location and engine thrust) to satisfy the specified mission constraints; and (vi) minimize MTOGW with respect to the engine thrust and repeat the previous steps if the low-boom objective value for the optimized thrust is too high or there is any mission constraint violation.

A theoretical rationale for such a decomposition method is the following. Suppose that an ideal optimal solution exists with the A_e matching error = 0. Then

$$A^{\text{lift}}_{\text{new,e}}(x_e) + A^{\text{volume}}_{\text{new,e}}(x_e) = A_{\text{new,e}}(x_e) = A^{\text{target}}_{\text{new,e,r}}(x_e) \quad \text{for } 0 \le x_e \le x_{\text{new,limit}} \tag{10}$$

If both the wing and fuselage design variables are used to reduce the A_e matching error, an optimizer might not know that it is usually more desirable to use the lift distribution than the fuselage width distribution for a reduction of the A_e matching error. The separation of wing/tail lift tailoring and fuselage volume shaping helps minimize unnecessary fuselage width changes for the low-boom design. The wing/tail lift tailoring focuses on reducing the major trend differences (defined by Eq. (4)) between the $A_{e,r}$ target and A_e of the design, while the fuselage width shaping aims at reducing the average differences (defined by Eq. (5)) between the $A_{e,r}$ target and A_e of the design. Because the feasibility of the low-boom trim constraint generally implies the feasibility of the cruise SM constraint, only the trim constraint is required to ensure a feasible relationship between the longitudinal CG of the aircraft and aerodynamic pressure center at the start cruise condition. Once a plausible low-boom design with a feasible trim constraint value is generated, the remaining mission constraints can be enforced by a straightforward feasibility optimization using the auxiliary design variables (excluding the main gear longitudinal location and engine thrust).

The aircraft component arrangement limits the main gear longitudinal location. Empirical data are usually available for a good initial guess of the required thrust; then a design exploration is helpful to ensure that thrust and propulsion system parameters are optimized to minimize the MTOGW and meet the LTO constraints with LTO noise as a consideration.

III. Numerical Results

The decomposition method given in Subsection II.F is successfully applied to find a plausible low-boom design that satisfies the ten mission constraints given in Subsection II.A. The following subsections document how the low-boom design is generated.

A. Baseline Configuration

The baseline geometry is given in Subsection II.E and the values for the auxiliary design variables are listed in Table 1. The main gear longitudinal location is set at x = 176 ft based on the geometry layout. The initial values for the remaining auxiliary design variables in Table 1 are inherited from preliminary design optimization runs. They have marginal effects on the low-boom design objective and low-boom trim margin. The following are the ten constraint values for the baseline.

(III.A.1) Low-boom trim margin = 0.16 ft (infeasible value)
(III.A.2) Main landing gear location constraint = 17.3 ft
(III.A.3) Cruise static margin for the low-boom mission = 16.8%
(III.A.4) Takeoff static margin = 1.5% (infeasible value)
(III.A.5) Landing static margin = 3.5%
(III.A.6) Takeoff field length = 7,482 ft
(III.A.7) Landing field length = 6,867 ft
(III.A.8) Tail rotation angle for trim at takeoff = -11.3°
(III.A.9) Tail rotation angle for trim at landing = -7.8°
(III.A.10) Approach velocity = 128 knots

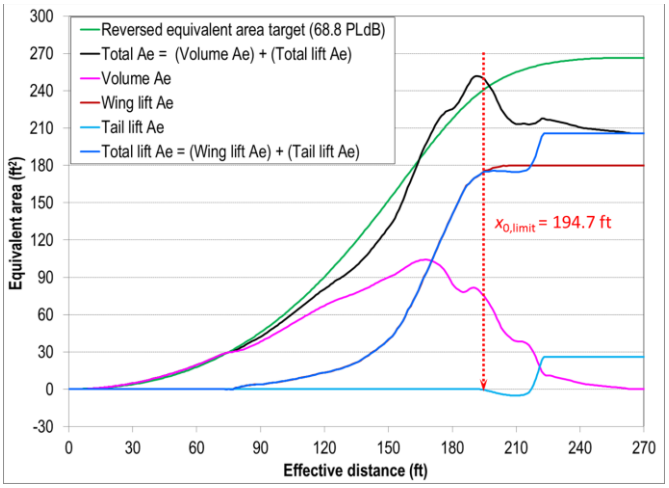

Fig. 7 A_e distributions for baseline.

The A_e distribution of the baseline differs significantly from its low-boom target over the specified effective distance interval from 0 ft to $x_{0,limit}$ = 194.7 ft (cf. Fig. 7). Note that the location where volume A_e starts to deviate from the low-boom $A_{e,r}$ target determines the longitudinal location of the LE of the root airfoil of the wing. The dash vertical line in Fig. 7 shows the location of $x_{0,limit}$ used in Eq. (3) for target scaling. Enough design variables are used to ensure that the baseline given in Fig. 6 has the lift tailoring authority to reduce the A_e differences between the baseline and target from x_e = 0 ft to x_e = 194.7 ft.

B. Lift Tailoring

Lift tailoring with the 24 wing and horizontal tail design variables is very effective to reduce the maximum A_e matching error while maintaining the low-boom trim margin of 1 ft. Initially, when the design variable ranges are large and/or there is no knowledge about how to avoid mission analysis failures with appropriate bounds on the design variables, the Non-Dominant Sorting Genetic Algorithm II in ModelCenter [32] is used for optimization. Later, when relatively small ranges for the design variables are used and mission analysis failures become rare, the Design Explorer in ModelCenter (cf. Section XI in Ref. [25]) is used for optimization. Between two successive optimization runs, the optimal solution of the first optimization run is used as the baseline design for the next optimization run and the ranges of the design variables are updated to set each baseline design variable near the mid location of the design range if possible. (In the literature, the choices of a baseline, its design variables, and their bounds are usually treated as a routine setup of an optimization problem. In practice, the usefulness of an optimization solution depends more on the problem setup than the optimization algorithm used to solve the problem.) The final optimization solution is obtained using the Design Explorer (for efficiency). The A_e distributions of the lift tailoring optimization solution are shown in Fig. 8. The wing shape changes are illustrated in Fig. 9. Note that the z-axis is magnified 5 times to provide a better view for airfoil changes. The most visible changes are a reduction of the wing span from 98 ft to 92 ft and more aft position of the tip airfoil.

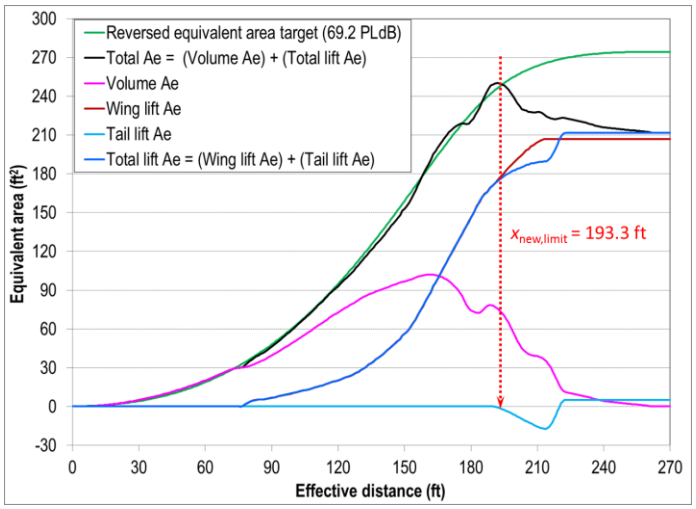

Fig. 8 A_e distributions for lift tailoring solution.

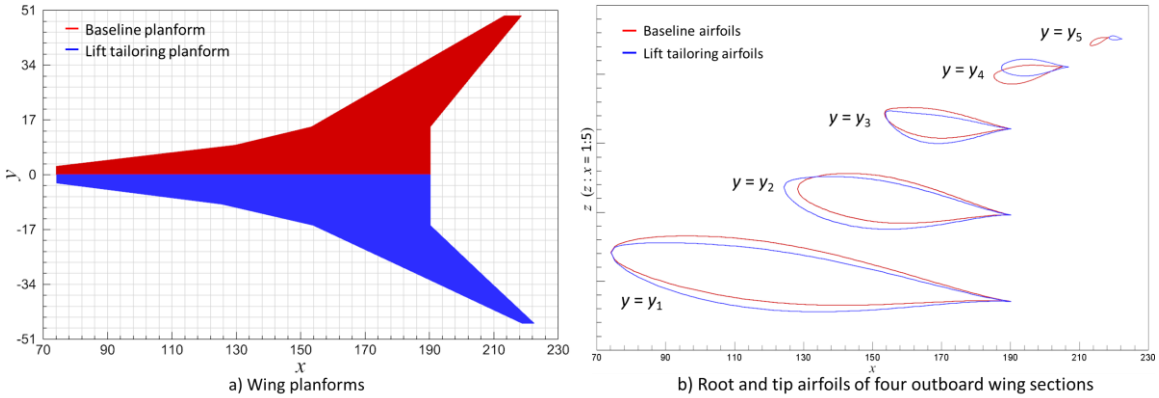

Fig. 9 Wing shapes of baseline and lift tailoring solution.

C. Fuselage Volume Shaping

The low-boom objective defined by Eq. (5) can be further reduced by fuselage volume shaping. The fuselage volume shaping problem is relatively easy to solve because the fuselage width changes rarely cause a mission analysis failure. The A_e distributions and A_e difference ($A_{new,e,r}^{target} - A_{new,e}$) are plotted in Fig. 10. The final optimization solution is obtained using the Design Explorer. The fuselage width comparison is shown in Fig. 11.

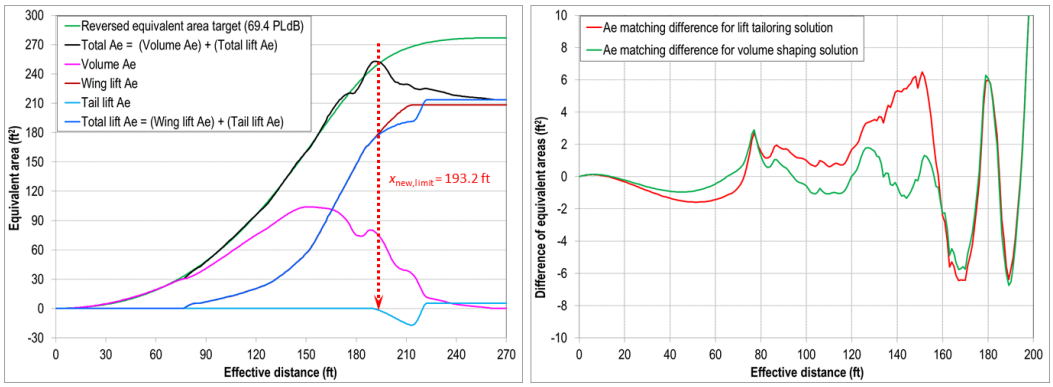

a) Equivalent areas for fuselage volume shaping solution b) A_e matching improvement by volume shaping

Fig. 10 Reduction of A_e matching error by fuselage volume shaping solution.

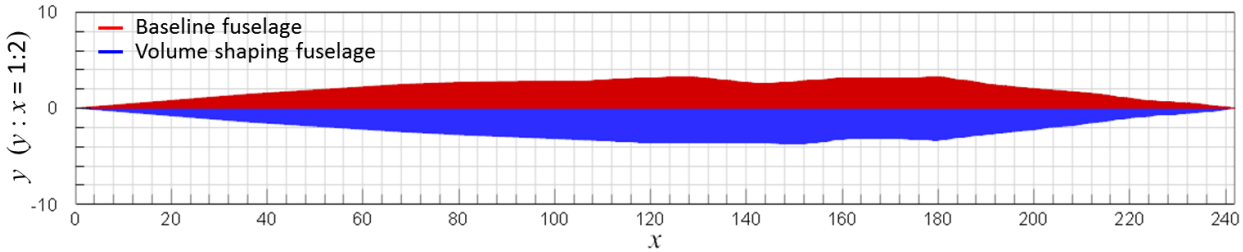

Fig. 11 Fuselage width distributions of baseline and volume shaping solution.

D. Low-Boom Optimization

Finally, run the low-boom design optimization for all geometry design variables with relatively small ranges for the design variables to reduce the low-boom design objective defined by Eq. (5). In this case, the number of design variables is too high for the Design Explorer. The Non-Dominant Sorting Genetic Algorithm II in ModelCenter is used to find the optimal solution of the low-boom optimization problem with the trim constraint for 35 shape design variables. After 77 hours of wall time (using a mix of desktop computers, Windows servers, and Linux servers), the genetic optimization algorithm terminates when reaching the maximum number (10,000) of iterations.

Table 2 Geometry design variables and their bounds for low-boom optimization solution

Wing camber	$0 \le \delta_{1,max} = 0.0004 \le 0.1$	$0 \le \delta_{2,max} = 0.004 \le 0.25$	$0 \le \delta_{3,max} = 0.132 \le 0.2$
	$0 \le \delta_{4,max} = 0.03 \le 0.2$	$0 \le \tau_{1,max} = 0.06 \le 0.2$	$0 \le \tau_{2,max} = 0.11 \le 0.25$
	$0 \le \tau_{3,max} = 0.22 \le 0.25$	$0 \le \tau_{4,max} = 0.0 \le 0.2$	$-5 \le \theta_4 = -1.7 \le -1$
	$-2 \le \theta_5 = 1.1 \le 2$		
Wing planform	$6 \le s_2 = 6.5 \le 7$	$5.9 \le s_3 = 6.5 \le 6.6$	$14.5 \le s_4 = 15.8 \le 17$
	$13 \le s_5 = 14.7 \le 15.6$	$115.4 \le c_1 = 116.3 \le 116.8$	$61.9 \le c_2 = 64.9 \le 66.9$
	$36.2 \le c_3 = 36.6 \le 38.2$	$3.4 \le c_5 = 4.2 \le 5.7$	$219 \le x_{tip} = 219.1 \le 224$
Horizontal tail	$16 \le$ span $= 18.1 \le 19$	$47 \le$ sweep $= 50.4 \le 52$	$27 \le c_{root} = 28.8 \le 31$
	$4 \le c_{tip} = 9.3 \le 11$	$-4 \le \theta_{htail} = -3.3 \le 0$	
Fuselage width	$65.3 \le x_1 = 68.2 \le 70.1$	$101.6 \le x_2 = 108.1 \le 113.7$	$118.6 \le x_3 = 124.5 \le 128.3$
	$147.6 \le x_4 = 154.1 \le 157.3$	$4.5 \le d_1 = 4.85 \le 5.5$	$5.4 \le d_2 = 6.78 \le 7.2$
	$5.58 \le d_3 = 7.25 \le 7.44$	$5 \le d_4 = 7.50 \le 8.5$	$6.3 \le d_5 = 6.30 \le 7.6$
	$6.3 \le d_6 = 6.75 \le 7.6$	$4.5 \le d_7 = 5.15 \le 5.5$	

The ranges and values of the design variables for the low-boom optimization solution are listed in Table 2. Recall that the design variable bounds are not known *a priori* and determined by successive optimization runs with empirical adjustments of the bounds. The basic rule is that the optimal design variable should not attain any specified upper or lower bound if the bound is not determined by the volume constraints for the cabin and main gear packaging.

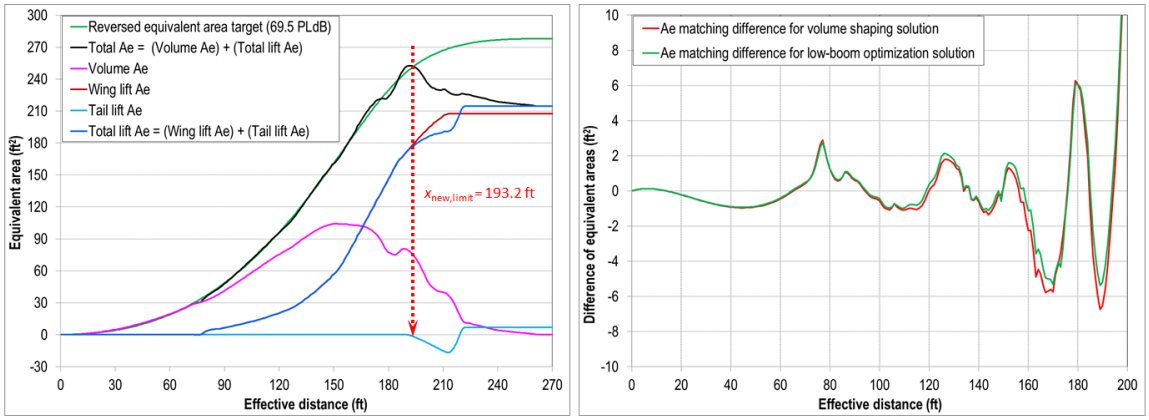

a) Equivalent areas for low-boom optimization solution b) A_e matching improvement by low-boom optimization

Fig. 12 Reduction of A_e matching error by low-boom optimization solution.

Figure 12 shows the A_e distributions and A_e difference ($A_{new,e,r}^{target} - A_{new,e}$) for the low-boom optimization solution. Only marginal matching error reduction is achieved as shown in Fig. 12 b). This indicates that the separation of lift tailoring and volume shaping does not lead to a severe penalty for minimizing the low-boom objective under the trim constraint. The lower width bounds for the cabin defined in Eq. (9) are relaxed for a better reduction of the A_e matching error. But, the optimal width parameters are large enough to maintain sufficient fuselage volume for 40 passenger seats and storage of main gear.

E. Feasibility Optimization

The six auxiliary design variables have almost no effect on the A_e matching error. The bounds of the design variables and values for the feasibility optimization solution are listed in Table 3. The objective function is the least square sum of the deflection angles and CG offsets.

Table 3 Auxiliary design variables and their bounds for feasibility optimization solution

Engine thrust = 49,000 lb	0 ≥ LE flap deflection angle for landing = -0.1 ≥ -2
Main gear longitudinal location = 176 ft	0 ≤ TE flap deflection angle for landing = 7.0 ≤ 13
10.5 ≤ Main gear length = 10.7 ≤ 11.4	0 ≤ Longitudinal CG offset for takeoff = 9.5 ≤ 11
0 ≤ TE flap deflection angle for takeoff = 5.7 ≤ 16	0 ≤ Longitudinal CG offset for landing = 9.1 ≤ 11

The following are the ten feasible constraint values for the feasibility optimization solution.

(III.E.1) Low-boom trim margin = 1.0 ft
(III.E.2) Main landing gear location constraint = 17.5 ft
(III.E.3) Cruise static margin for the low-boom mission = 16.4%
(III.E.4) Takeoff static margin = 2.0%
(III.E.5) Landing static margin = 2.0%
(III.E.6) Takeoff field length = 7,820 ft
(III.E.7) Landing field length = 7,995 ft
(III.E.8) Tail rotation angle for trim at takeoff = -11.6°
(III.E.9) Tail rotation angle for trim at landing = -8.9°
(III.E.10) Approach velocity = 143 knots

F. Engine Thrust Optimization

The decomposition method separates the design variables into weakly coupled groups and performs the optimization with respect to each group successively. The specified engine thrust based on a parametric study of the

baseline might not be optimal for the low-boom design. So the MTOGW of the low-boom design is minimized again with respect to the engine thrust. The optimal engine thrust is 47,950 lb. The minor change of the engine thrust has a negligible effect on the low-boom characteristics; the two low-boom designs for engine thrusts of 49,000 lb and 47,950 lb have nearly identical A_e distributions (cf. Fig. 13).

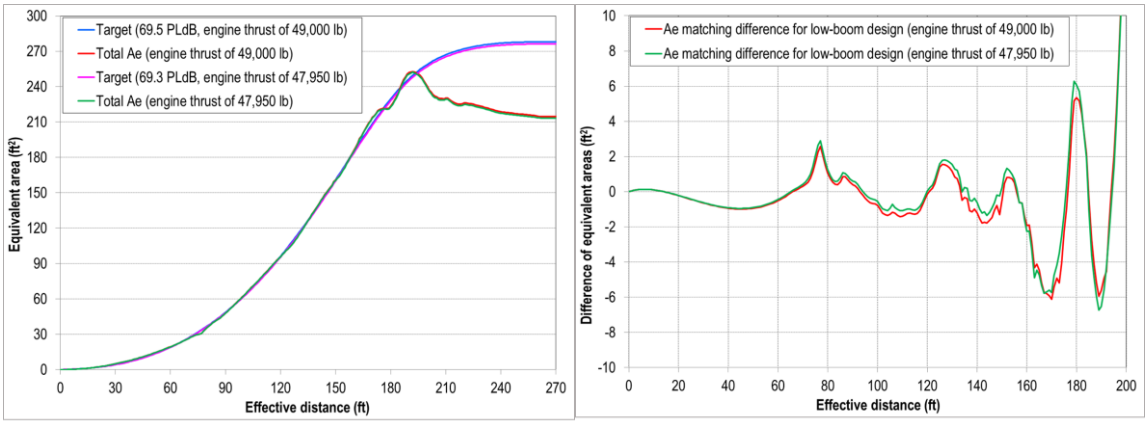

a) $A_{e,r}$ targets and A_e distributions b) A_e matching differences

Fig. 13 Comparison of low-boom solutions for engine thrusts of 49,000 lb and 47,950 lb.

The low-boom design for engine thrust of 47,950 lb also satisfies the ten mission constraints.

(III.F.1) Low-boom trim margin = 1.05 ft ≥ 1 ft
(III.F.2) Main landing gear location constraint = 17.5 ft ≥ 4 ft
(III.F.3) Cruise static margin for the low-boom mission = 16.5% ≥ 2%
(III.F.4) Takeoff static margin = 2.1% ≥ 2%
(III.F.5) Landing static margin = 2.0% ≥ 2%
(III.F.6) Takeoff field length = 7,897 ft ≤ 8,300 ft
(III.F.7) Landing field length = 7,962 ft ≤ 8,300 ft
(III.F.8) Tail rotation angle for trim at takeoff = -11.5° ≥ -20°
(III.F.9) Tail rotation angle for trim at landing = -9.0° ≥ -20°
(III.F.10) Approach velocity = 143 knots ≤ 150 knots

Table 4 gives a weight comparison of these two low-boom designs. The weight differences are negligible. The successive low-boom optimizations do not significantly change the optimality of the specified engine thrust of 49,000 lb determined by a parametric study of the engine thrust for the baseline.

Table 4 Weight comparison of two low-boom designs

	Low-boom MTOGW	Overwater MTOGW	Zero fuel weight
Low-boom design for engine thrust of 49,000 lb	200,493 lb	192,756 lb	100,694 lb
Low-boom design for engine thrust of 47,950 lb	199,334 lb	193,240 lb	100,543 lb

G. Re-optimization for Requirement Change

For aircraft conceptual design, it happens often that some critical assumptions for the design problem were found to be incorrect after the design problem had been solved successfully. An updated economic feasibility study of the previously generated low-boom supersonic transport shows that the low-boom supersonic configuration would be economically viable if it could have better aerodynamic performance and fly the overwater mission for 3,600 nm. The previous low-boom configuration with engine thrust of 47,950 lb can carry an additional 6,093 lb of fuel to reach the maximum allowed MTOGW for the overwater mission (cf. Table 4) and increase its overwater range to 3,402 nm; but this does not meet the new requirement for overwater range of 3,600 nm. So the configuration is redesigned with the 3,600 nm overwater-range constraint. In an attempt to improve aerodynamic performance, the wing span is constrained to be as short as possible. After applying the decomposition method multiple times, the final design is a much lighter low-boom supersonic aircraft (with MTOGW = 157,583 lb) that flies 3,600 nm (instead of 3,200 nm) overwater at cruise Mach 1.8. The corresponding low-boom target has an undertrack ground noise level of 67.8 PLdB. Past experiences show that a margin of 5 PLdB for the low-boom target is adequate to derive a CFD-based low-boom

design from a low-fidelity low-boom design; that is, if a low-fidelity design matches a low-boom target of less than 70 PLdB, then it could be further refined as a CFD-based design with an undertrack ground noise level less than 75 PLdB. The lower noise level of 67.8 PLdB shows that there is some excess margin for the low-boom target and a shorter vehicle might still be able to satisfy the low-boom requirement. So a re-optimization iteration begins to shorten the aircraft length to 232 ft. Such design iterations for changing assumptions and requirements are typical for low-boom aircraft conceptual design. The re-optimization solution satisfies all the specified mission constraints and has a lower MTOGW than the previous low-boom design with fuselage length of 242 ft. Figure 14 a) shows the A_e distributions of the re-optimization solution; Figures 14 b) and c) compare the wing planforms and fuselage width distributions, respectively, of the two low-boom designs with two different overwater-range constraints. The fuselage width distribution of the re-optimization solution has a minimum width of 5.5 ft, but it still has enough volume for 40 passengers and storage of main gear (cf. Fig. 15, where the pilots and passengers are imported from an Uber eVTOL common reference model [33]).

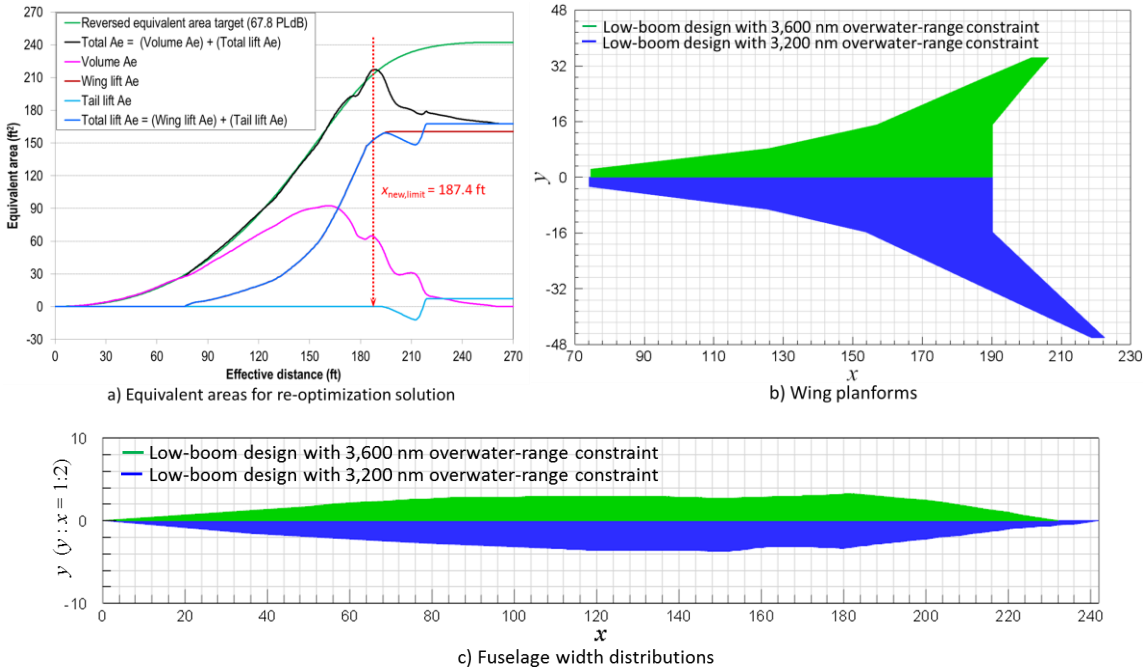

Fig. 14 A_e distributions and shape changes for re-optimization solution.

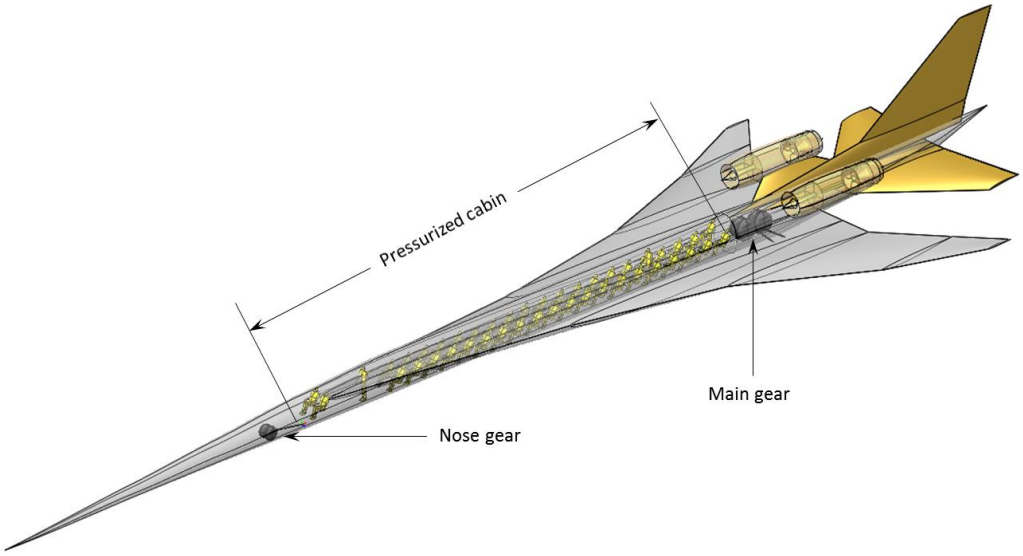

Fig. 15 Cabin arrangement and main gear packaging for re-optimization solution.

The ten mission constraint values for the re-optimization solution are the following.

(III.G.1) Low-boom trim margin = 3.69 ft ≥ 1 ft
(III.G.2) Main landing gear location constraint = 13.1 ft ≥ 4 ft
(III.G.3) Cruise static margin for the low-boom mission = 18.0% ≥ 2%
(III.G.4) Takeoff static margin = 2.1% ≥ 2%
(III.G.5) Landing static margin = 2.0% ≥ 2%
(III.G.6) Takeoff field length = 8,280 ft ≤ 8,300 ft
(III.G.7) Landing field length = 8,003 ft ≤ 8,300 ft
(III.G.8) Tail rotation angle for trim at takeoff = -6.6° ≥ -20°
(III.G.9) Tail rotation angle for trim at landing = -6.0° ≥ -20°
(III.G.10) Approach velocity = 150 knots ≤ 150 knots

Table 5 compares some specifications of the two low-boom designs with two different overwater-range constraints. It is obvious *now* that the low-boom design with the 3,200 nm overwater-range constraint would have a much lower MTOGW if the wing span were constrained properly and simultaneous minimization of the low-boom objective and MTOGW were performed. Note that the wing span of 98 ft of the baseline (cf. Fig. 6) was based on previous design exploration results; the low-boom MDO runs in the previous subsections searched for an optimal low-boom solution with the specified mission constraints in a design space around the baseline, which did not include configurations with spans as short as 69 ft. Applications of knowledge gained during successive MDO runs eventually lead to a much lighter low-boom design for the overwater range of 3,600 nm. The MTOGW reduction is mainly due to the reductions of wing span, engine thrust, and fuselage length. A further reduction of the engine thrust could lead to a lower MTOGW, but it would require a maximum takeoff field length more than 8,300 ft. The re-optimization process is terminated by the constraint for maximum takeoff field length of 8,300 ft. A further reduction of the fuselage length is not possible because of the cabin length and component layout restrictions, unless that the longitudinal seat spacing of 4 ft is reduced. Therefore, this low-boom concept is considered to be optimal for the specified longitudinal seat spacing of 4 ft, maximum takeoff field length of 8,300 ft, low-boom cruise Mach 1.6 for a range of 2,500 nm at cruise altitude of 45,000 ft, overwater cruise Mach 1.8 for a range of 3,600 nm at cruise altitude of 60,000 ft, and low-boom undertrack ground noise level less than 75 PLdB. Any change of these requirements/assumptions could potentially lead to significant changes of the resulting low-boom concept.

Table 5 Comparison of two low-boom designs with two different overwater-range constraints

	Overwater range of 3,200 nm	Overwater range of 3,600 nm
Engine thrust	47,950 lb	36,700 lb
Fuselage length	242 ft	232 ft
Wing span	92 ft	69 ft
Wing area	3,678 ft^2	3,009 ft^2
Zero fuel weight	100,543 lb	76,249 lb
Low-boom MTOGW	199,334 lb	154,474 lb
Overwater MTOGW	193,240 lb	153,212 lb

IV. Concluding Remarks

The decomposition method for the low-boom MDO problem with the specified mission constraints is successfully applied to generate a low-boom supersonic transport for 40 passengers at a cruise Mach of 1.6 with a range of 2,500 nm. The generated low-boom configuration can also perform an overwater mission at cruise Mach 1.8 for a range of at least 3,600 nm. The remaining ten mission constraints include the low-boom trim constraint and static margins for takeoff/cruise/landing, etc. A total of 43 design variables are used for MDO, including the engine thrust, main gear length, wing and horizontal tail shape parameters, and fuselage cross section widths and locations. The volume constraints for 40 passengers and main gear packaging are enforced by the lower bounds on the fuselage width design variables. The most difficult challenge is to resolve the conflict between attaining a desirable low-boom design objective and maintaining the aircraft longitudinal CG ahead of the aerodynamic center of pressure at the start cruise condition of the low-boom mission. The latter constraint is referred to as the low-boom trim constraint. The low-boom design objective and low-boom trim constraint are both mainly determined by the volume and lift distributions of the configuration. Finding the best compromise between them is a difficult optimization problem, which might be unsolvable. Furthermore, potential mission analysis failures due to insufficient thrust and/or poor aerodynamic performance make the objective and constraint functions of the low-boom MDO problem discontinuous, effectively

forcing the use of genetic optimization algorithms for an optimal solution. Even if there exists a feasible solution for the low-boom MDO problem with the specified mission constraints, it is difficult to know *a priori* what design variables and their ranges are sufficient to obtain such a solution. The successful application of the decomposition method shows that such a difficult MDO problem is solvable.

It is well known that low-fidelity aerodynamics and CFD yield totally different lift distributions for a supersonic configuration. A natural question is whether the feasibility of a low-fidelity low-boom MDO problem can be retained using high-fidelity analyses. A theoretical hypothesis with empirical evidence is provided in Section I to justify why matching the low-fidelity equivalent area distribution to a reversed equivalent area target could lead to a CFD-based low-boom design satisfying the same mission constraints. Moreover, the calibration of empirical aircraft weights estimation by FEA-based wing and fuselage weight estimates in Subsection II.D shows that the weights and CGs could be calculated using a multifidelity approach so that they are consistent with FEA-based analysis results. The consistency between low-fidelity and high-fidelity aerodynamic performance analyses will be studied in the future.

In conclusion, the proposed low-fidelity low-boom MDO method is calibrated with CFD/FEA analyses; it has been used to generate a low-boom configuration that satisfies all the specified mission constraints and has the potential to attain a low-boom ground noise level below 75 PLdB. Moreover, the existence of such a low-fidelity low-boom design implies the feasibility of a CFD/FEA-based low-boom design with the same mission constraints.

Acknowledgments

This work is funded by the NASA Commercial Supersonic Technology Project and Transformational Tools & Technologies Project.

References

[1] Li, W., Campbell, R., Geiselhart, K., Shields, W., Nayani, S., and Shenoy, R., "Integration of Engine, Plume, and CFD Analyses in Conceptual Design of Low-Boom Supersonic Aircraft," AIAA Paper 2009-1171, June 2009.

[2] Ordaz, I., and Li, W., "Integration of Off-Track Sonic Boom Analysis in Conceptual Design of Supersonic Aircraft," AIAA Paper 2011-464, June 2011.

[3] Ordaz, I., Li, W., and Campbell, R., "Automated Tetrahedral Mesh Generation for CFD Analysis of Aircraft in Conceptual Design," AIAA Paper 2014-0118, June 2014.

[4] Park, M., and Nemec, M., "Nearfield Summary and Statistical Analysis of the Second AIAA Sonic Boom Prediction Workshop," AIAA Paper 2017-3256, June 2017.

[5] Li, W., and Rallabhandi, S. K., "Inverse Design of Low-Boom Supersonic Concepts Using Reversed Equivalent-Area Targets (Invited)," AIAA Paper 2011-3498, June 2011. *Journal of Aircraft*, Vol. 51, No. 1, 2014, pp. 29–36.

[6] Ordaz, I., and Li, W., "Adaptive Aft Signature Shaping of a Low-Boom Supersonic Aircraft Using Off-Body Pressures," AIAA Paper 2012-0020, January 2012.

[7] Ordaz, I., Geiselhart, K., and Fenbert, J., "Conceptual Design of Low-Boom Aircraft with Flight Trim Requirement," *Journal of Aircraft*, Vol. 52, No. 3, 2015, pp. 932–939.

[8] Li, W., "Feasibility of Supersonic Aircraft Concepts for Low-Boom and Flight Trim Constraints," AIAA Paper 2015-2581, June 2015.

[9] Ueno, A., Kanamori, M., and Makino, Y., "Multi-fidelity Low-boom Design Based on Near-field Pressure Signature," AIAA Paper 2016–2033, January 2016.

[10] Aftosmis, M., Nemec, M., and Cliff, S., "Adjoint-Based Low-Boom Design with Cart3D (Invited)," AIAA Paper 2011-3500, June 2011.

[11] Wintzer, M., Ordaz, I., and Fenbert, J., "Under-Track CFD-Based Shape Optimization for a Low-Boom Demonstrator Concept," AIAA Paper 2015-2260, June 2015.

[12] Mack, R., "A Supersonic Business-Jet Concept Designed for Low Sonic Boom," NASA TM-2003-212435, October 2003.

[13] Geiselhart, K., Ozoroski, L., Fenbert, J., Shields, E., and Li, W., "Integration of Multifidelity Multidisciplinary Computer Codes for Design and Analysis of Supersonic Aircraft," AIAA Paper 2011-0465, January 2011.

[14] Hamel, L., Folk, T., Jimenez, H., and Mavris, D., "Conceptual Design of an N+2 Supersonic Airliner," AIAA Paper 2009-7075, September 2009.

[15] Morgenstern, J., Norstrud, N., Stelmack, M., and Jha, P., "Advanced Concept Studies for Supersonic Commercial Transports Entering Service in 2030-2035 (N+3)," AIAA Paper 2010-5114, June 2010.

[16] Morgenstern, J., Norstrud, N., Sokhey J., Martens, S., and Alonso, J., "Advanced Concept Studies for Supersonic Commercial Transports Entering Service in the 2018 to 2020 Period," NASA CR-2013-217820, February 2013.

[17] Welge, H., Bonet, J., Magee, T., Tompkins, D., Britt, T., Nelson, C., Miller, G., Stenson, D., Staubach, J., Bala, N., Duge, R., O'Brien, M., Cedoz, R., Barlow, A., Martins, S., Viars, P., Rasheed, A., Kirby, M., Raczynski, C., Roughen, K., Doyle, S., Alston, K., Page, J., and Plotkin, K., "N+3 Advanced Concept Studies for Supersonic Commercial Transport Aircraft Entering Service in the 2030-2035 Period," NASA CR-2011-217084, April 2011.

[18] Magee, T., Fink, L., Fugal, S., Adamson, E., and Shaw, S., "Boeing N+2 Supersonic Experimental Validation Phase II Program," AIAA Paper 2014-2137, June 2014.

[19] Alonso, J., LeGresley, P., and Pereyra, V., "Aircraft Design Optimization," *Mathematics and Computers in Simulation*, Vol. 79, No. 6, 2009, pp. 1948–1958.
[20] Choi, S., Alonso, J., Kroo, I., and Wintzer, M., "Multifidelity Design Optimization of Low-Boom Supersonic Jets," *Journal of Aircraft*, Vol. 45, No. 1, 2008, pp. 106–118.
[21] Mathieu, M., Marin, A., Stephenson, K., Beard, J., Castillo, E., Weddle-Weaver, C., Teni, D., and Takahashi, T., "Preliminary Design of an N+1 Overwater Supersonic Commercial Transport Aircraft, AIAA Paper 2017-1387, June 2017.
[22] Phillips, B., and West, T., "Trim Flight Conditions for a Low-Boom Aircraft Design Under Uncertainty," *Journal of Aircraft*, Vol. 56, No. 1, 2019, pp. 53–67.
[23] Kasuga, Y., and Yoshida, K., "A New F-Function for the Low-Boom Aircraft Design with Trim Requirement," AIAA Paper 2016-2032, January 2016.
[24] Mack, R., and Kuhn, N., "Determination of Extrapolation Distance with Measured Pressure Signatures from Two Low-Boom Models," NASA TM-2004-213264, November 2004.
[25] Ozoroski, L., Geiselhart, K., Padula, S., Li, W., Olson, E., Campbell, R., "Initial Multidisciplinary Design and Analysis Framework," NASA TM-2010-216711, June 2010.
[26] Li, W., Geiselhart, K., Olson, E., and Robinson, J., "Automation of Structural Sizing of Aircraft Concepts Under Static Aeroelastic Constraints," AIAA Paper 2018-0103, January 2018.
[27] Wells, D., Horvath, B., and McCullers, L., "The Flight Optimization System Weights Estimation Method," NASA TM-2017-219627, Volume 1, January 2017.
[28] Mccullers, L., "FLOPS User Guide," NASA Langley Research Center, Hampton, Virginia, 2008.
[29] OpenVSP, Version 3.16.1, Open Source, URL:http://www.openvsp.org [retrieved 9 July 2019].
[30] Candel, S., "Concorde and the Future of Supersonic Transport," *Journal of Propulsion and Power*, Vol. 20, No. 1, 2004, pp. 59–68.
[31] Ladson, C., Brooks Jr., C., Hill, A., and Sproles, D., "Computer Program to Obtain Ordinates for NACA Airfoils," NASA TM-1996-4741, December 1996.
[32] ModelCenter, Version 11.2, Phoenix Integration Inc., URL:http://www.phoenix-int.com [retrieved 9 July 2019].
[33] Uber eVTOL common reference models, https://www.uber.com/us/en/elevate/uberair/ [retrieved 9 July 2019].